Nanoscale

Accepted Manuscript

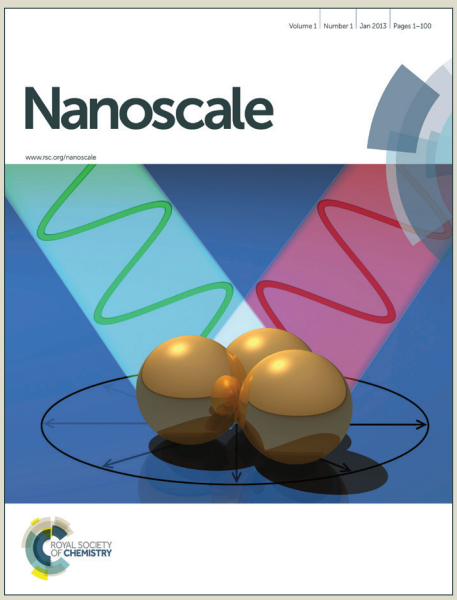

ROYAL SOCIETY OF CHEMISTRY

www.rsc.org/nanoscale

Predictive of the Quantum Capacitance Effect on the Excitation of Plasma Waves in Graphene Transistors with Scaling Limit

Lin Wang*, Xiaoshuang Chen*, Yibin Hu, Shaowei Wang and Wei Lu

National Laboratory for Infrared Physics, Shanghai Institute of Technical Physics, Chinese Academy of Sciences, 500 Yu Tian Road, Shanghai, Shanghai 200083, China

Synergetic Innovation Center of Quantum Information & Quantum Physics, University of Science and Technology of China, Hefei, Anhui 230026, China

*Address correspondence to wanglin@mail.sitp.ac.cn; xschen@mail.sitp.ac.cn;

Plasma waves in graphene field-effect transistors (FETs) and nano-patterned graphene sheets have emerged to be very promising candidate for potential terahertz and infrared applications in myriad areas including remote sensing, biomedical science, military, and many other fields with ability of electrical tunable and strong interaction with light. In our work, we study the excitations and propagation properties of plasma wave in nanometric graphene-FET down to the scaling limit. Due to the quantum-capacitance effect, the plasma wave exhibits strong correlation with the distribution of density of state (DOS). It is indicated that the electrical tunable plasma resonance has the power-dependent $V_{TG}^{0.8}$ relation on the gate voltage, which is originated from the linear dependence of density of states (DOS) on the energy in pristine graphene, in striking different from those dominated by the classical capacitance with only $V_{TG}^{0.5}$ dependence. The results of different transistor-sizes indicate the potential application of nanometric graphene FETs in highly-efficient electro-optic modulation or detection of terahertz or infrared radiation. In addition, we highlight the perspectives of plasma resonance excitation in probing the many-body interaction and quantum matter state in strong correlation electron system. This study reveals the key feature of plasma wave in decorated/nanometric graphene FETs, and paves the way to tailor the plasma band-engineering and expand its application in both terahertz and mid-infrared regions.

KEYWORDS: quantum capacitance· plasma waves· many-body effect· Boltzman theory · strong correlation

Quantum capacitance has been found to have an important role in the quantum behavior of electron gas systems, such as strong correlated interaction[1], resonance impurities[2], electron-hole asymmetry[3], in particular the electron density of state (DOS) distributions which are affected both by single-particle and many-body interactions[4]. It is especially instructive for two-dimensional electron system with the global electron density reversibly tuned by the electrostatic gating. The quantum capacitance has originally been suggested to explain the extra capacitance observed in III-V high electron mobility transistors (HEMTs) with discrete energy levels under strong inversion regime[5]. Recently, the rise of semiconducting 2D crystals has given much more opportunity for effectively exploring the unexpected physical behavior, such as conductivity anomaly, fractional quantum-Hall phase transition, and Fermi-velocity renormalization[1, 6-10]. Among them, graphene, a single-layer carbon atom with 2D honeycomb lattice, has stimulated most extensive experimental and theoretical investigations due to its intrinsic high carrier mobility and clear relevance for technological application in photonics, electronics and plasmonics[11].

However, the understanding of mesoscopic-physical behavior in graphene is still far from completed and the quantum capacitance becomes nontrivial when the vertical scaling down of the graphene FETs is continued.

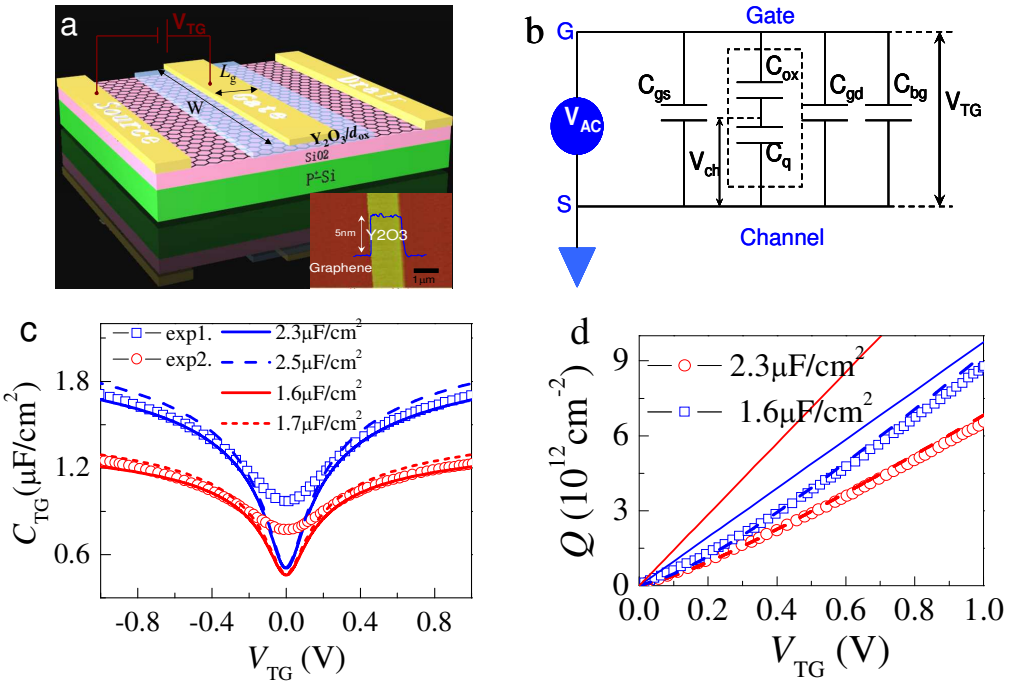

Fig. 1. Experimental and theoretical results of quantum-capacitance in graphene FETs. (a) Schematic of graphene FET with 4nm and 6nm Y_2O_3 top-gate dielectric layers (seeing Methods section) investigated in this work, respectively. The channel area covered by the top gate is with width W=5μm, length L_g=7μm, the separation from source/drain to the top-gate is 1μm. Inset displays the AFM topography of Y_2O_3/Graphene. (b) The equivalent circuit of capacitance bridge technique for quantum capacitance measurements of graphene FET, G, S, and D stand for gate, source and drain ends, respectively. (c) Comparison of top-gated capacitances under different gate voltages between experiments (symbols) and theories with different oxide capacitances C_{ox} (dashed and solid lines), the results are in well agreement above the Dirac point. (d) Sheet carrier density versus gate voltage V_{TG} after integration of C_{TG}-V_{TG} results in (c), solid lines are the theoretical results based on the parallel-plate capacitor model with only the oxide capacitance C_{ox}. Dashed lines are the theoretical results with quantum-capacitance correction, in well consistent with the experimental results in almost all bias range.

Unlike conventional 2D electron systems, the density of state of graphene depends linearly on the energy, subsequently resulting in the sensitive change of capacitance due to absence of DOS near the Dirac point even with the oxide-layer thicker than 50nm[9, 12]. While at higher carrier density, the occupation of split-off band leads to parallel transport channel, which is crucial for future applications in visible/near-infrared technologies. Therefore, sufficient gate control on the conduction channel is important to improve performance of graphene-FETs-based photodetectors and circuits[12]. To enable efficient coupling between gate electrode and transistor channel, the so-called ionic-liquid gates and high-k dielectric layers down to several ~nm are implemented [13, 14]. Especially, the ionic-liquid gating structures have been reported to continuously tune the carrier

density exceeding 10^{14}cm^{-2}. Meanwhile, the ionic gating of graphene-nanodisks has already exhibited inspiring plasmon-induced strong absorption at mid-infrared frequency with Fermi level tuned from 0.2eV up to 0.8eV[10, 15]. Since a single sheet of homogeneous graphene absorbs only 2.3% of incident light in the visible and near-infrared range, the realization of both direct optical excitation and facile electrical tunability of plasmons in graphene nanostructures is greatly desired for improving device applicability. While due to small ion radius (over ~tens μF/cm^2) in liquid gate and thin-dielectric layer used[16], the quantum capacitance effect in nano-structured device would inevitably dominates the electrostatic doping efficiency of electron gas during the gate-voltage sweeping. Also it is not much clear about the role of such effect on the properties (e. g. electrical tunability) of plasma wave. Even though the presence of quantum capacitance will deteriorate the electrostatic doping, in this Letter, we find improved voltage-dependence of plasma waves in graphene FET through thinning the dielectric layer. With further analysis, it is indicated that the excitation of plasma wave is in strong correlation with the DOS distribution of graphene. In addition, the redistribution of DOS caused by the many-body interaction is detectable through observing the shift of plasma wave resonance or in other words, the dispersion of plasma wave can be tuned by changing electronic states.

The device considered in this work consists of a monolayer graphene on top of a SiO_2 (300nm)/Si substrate (Methods section). Fig. 1 depicts the geometry of top-gated graphene FETs with Y_2O_3 film serves as the gate dielectric stack grown on graphene via depositing a thin layer yttrium (Y) film by using electron-beam evaporation followed by thermal oxidation[2, 17]. The total gate capacitance is measured between electrode and channel with the setup of capacitance bridge technique[17] (Fig. 1b). Also, the RF technique can be applied for capacitance measurement but with less accurate and depends on selected model[18]. Both of these two methods are affected by the parasitic capacitance, i. e. C_M=C_{TG}+C_{gs}+C_{gd}+C_{bg}, C_M is the measured capacitance, C_{gs} (C_{gd}) and C_{bg} is the parasitic capacitance between the gate and source (drain), backgate, the total contribution of which is estimated by measurement without graphene and is around 3nF/μm^2. Differential capacitance C_{TG} can be described in the series of geometrical capacitance C_{ox} and quantum capacitance $C_Q \sim \frac{2e^2 k_B T}{\pi(\hbar v_F)^2}\ln\left[2\left(1+\cosh\frac{\mu}{k_B T}\right)\right]$ (μ is chemical potential, k_B is Boltzman constant and T is temperature) (Fig. 1(b)). All the curves in Fig. 1(c) display unusually minimum and peculiar "V-shape" near the Dirac point, where the quantum capacitance is especially important due to the absence of DOS in pristine graphene. The theoretical modeling results based on the assumption of graphene with linear DOS are shown in Fig. 1c in together with the experimental results (squares and circles). The best fitting is obtained when the oxide capacitances C_{ox} are 1.7μF/cm^2 and 2.3μF/cm^2, respectively. Therefore, the actual thickness of Y_2O_3 film in Fig. 1c is estimated around 6nm/ 4nm with deviation less than 1nm after considering the instability of oxidation process, in consistent with the atomic force microscopy results[2,17]. As referring to the quantum capacitance, the Fermi velocity v_F is assumed to be a constant~1.0×10^{8}cm/s with weakly dependence on density. The assumption is reasonable since the value of Fermi velocity has been tested numerously in optics and electronics, and it is found that the many-body contribution is negligible in Fig. 1a. Besides, near the Dirac point, the many-body effect is overwhelmed by the substrate disorder, which has been confirmed recently by magnetic transport measurement[1]. Therefore, the potential fluctuations caused by the residues near the interface between graphene

and substrate will give rise to the additional microscopic capacitance at the Dirac point. From Fig. 1d, it can be seen the low-DOS leads to the poor electrostatic doping and strong quantum capacitance in all bias-voltage ranges.

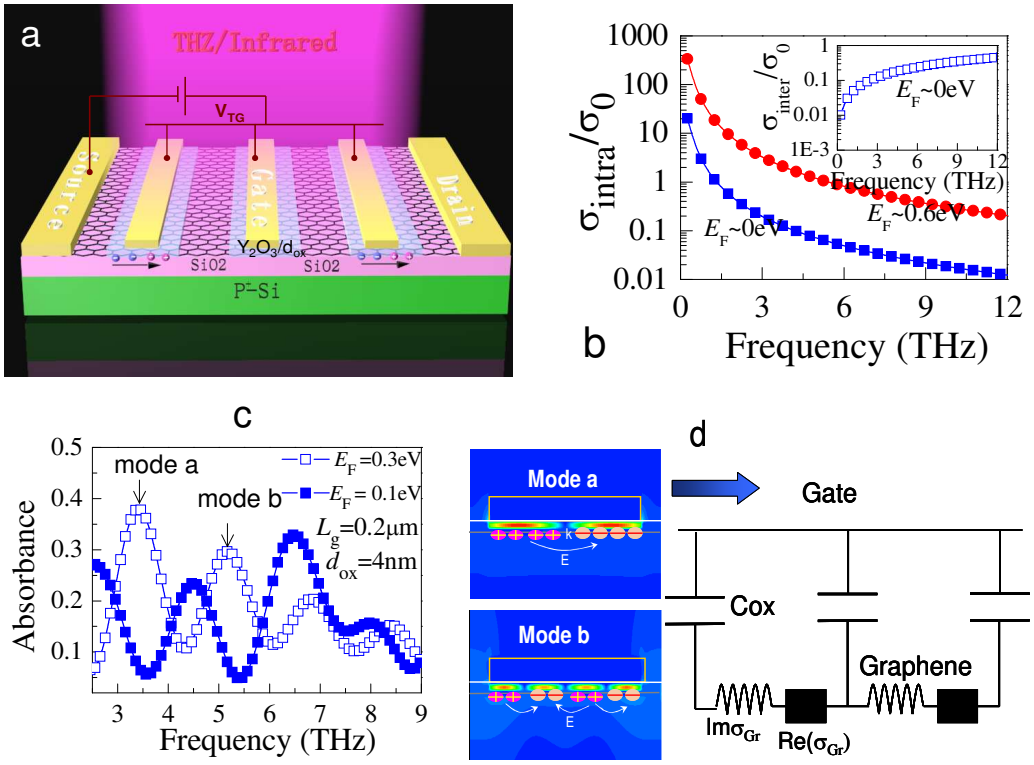

Fig. 2. Spectral characteristic of plasma wave in graphene FETs and its equivalent circuit model. (a)Sketch of one-dimensional periodic array of graphene plasma wave FETs under excitation by the THz/IR radiation. The plasma wave oscillations are depicted in the channel schematically. (b)The dynamical intra and inter-band conductivity of graphene based on the Kubo theory, inset indicates the energy loss ratio between intra-band and inter-band process at room temperature near the Dirac point, the imaginary part of conductivity is not shown in the figure, as it is dominated by the intraband conductivity, and thus the frequency of plasma waves in graphene FETs is mainly determined by the intraband part. (c) The spectral characteristic of plasma resonance in grating-gated graphene FET at Fermi level E_F~0.1eV (solid symbols) and E_F~0.3eV (open symbols) obtained by solving the Maxwell equations embedded with Kubo conductivity theory (seeing Supporting Informations). The gate length L_g is 0.2μm, and oxide layer thickness d_{ox} is 4nm. (d)Mode profiles of resonances a and b in (c), and the equivalent R-L-C model for plasma wave oscillation in the gated channel. It should be noted that the sheet conductance in local approximation is given by $\sigma W/L_g$, L_g is the gate length and W is the gate width, the capacitance is give by the CWL_g, the kinetic inductance is given by $\mathrm{Im}(1/\sigma)L_g/W$, which leads to the similar expression for plasma wave frequency as the Boltzman and RPA approximation theories in the Supporting Informations.

Based upon above discussed results, it is questionable on whether the electrical tunability of plasma resonances in graphene FETs can be improved when vertically scaling-down of dielectric layer continues. To this regard, we explore in details the effect of quantum capacitance on the

plasma resonance by employing rigorously plasmonic modeling technique (see Methods section and Supporting Informations), and try to pave an alternative way to investigate the mesoscopic physical behavior of 2DEG (two-dimensional electron gas). The prototype of graphene FETs is shown in Fig. 2a schematically, where multiple graphene transistors are connected in series. Under the THz radiation excitation, adjacent unit cells of FETs oscillate collectively in-phase, shrinking the THz field into the grating-gaps. Most part of the zeroth diffraction-order transmits into the substrate, and the plasma wave is excited by the higher-order evanescent field close to the gratings.

To investigate the properties of plasma wave in pristine-graphene FET, we solved self-consistently the Maxwell equations based on the FDTD methods (seeing Methods sections), during which the optical conductivity of graphene sheet is obtained by the both Kubo and RPA theories (seeing Supporting Information)[20]. In a pristine graphene, the change of optical transmission is mainly caused by the intraband ($\sigma_{intra}(\omega)$) or interband ($\sigma_{inter}(\omega)$) dynamical conductivity depending on the threshold condition[19]. The distributions of intraband and interband conductivities at terahertz region are plotted schematically in Fig. 2b, from where it can be seen that the intra-band Drude term can be orders of magnitude larger than the interband one, especially when the Fermi level is far from Dirac point. In different from the surface plasmon in graphene disks, array or graphene sheet, the plasma waves in FET interact strongly with the electrodes, and the image charges induced at the electrode screen the plasma oscillation in the graphene sheet. Because of this, the frequency of plasma wave follows the linear rather than square-root dispersion of its wavevector[21, 22](seeing Supporting Informations).

Figs. 2c and 2d display the absorption and field-profile induced by the plasma-wave oscillation in a periodic array of Y_2O_3/graphene transistor with 0.2μm gate length and 4nm dielectric layer under the illumination of THz radiation. In such thin-film graphene FET, the plasma wave oscillation in channel can be strongly suppressed due to the large damping constant τ_{RC} (τ_{RC}~$R_{ch}C_{ox}$) caused by the large shunt capacitance (Fig. 2d). Following the scheme of hydrodynamic theory developed by Dyakonov and Shur[23], the propagation constant of plasma wave is given by $\omega(1+i/\omega\tau)^{1/2}/s$. Therefore the effective propagation length L_{eff} of plasma waves along the channel of graphene is determined only by $s\tau$, where $s=(ne^2/m_C C_{ox})^{1/2}$ is plasma wave velocity, $s>10^8$cm/s (for more details, seeing Supporting Information). The length can be further rewritten as $L_g(\tau/\tau_{RC})^{1/2}$ (c. f. Fig. 2d, τ_{RC}~1×10^{-13}s). Due to the capacitive coupling between electrode and graphene-channel (Fig. 2d), the unit cell of graphene FET acts as a R-L-C oscillator (see Fig. 2d), compressing the THz radiation down to sub-micrometer dimensions. In addition, it is no doubt that the propagation length of plasma waves in graphene decreases when the thickness of Y_2O_3 is reduced.

To indicate more clearly the vertical scaling-limits of dielectric layer for efficient correlation between quantum capacitance and plasma oscillation, the sensitive changes of plasma resonance with the change of the device structure parameters are displayed **in Fig. 3 by applying FDTD simulations. It is discernable that the frequency of plasma resonance (which is corresponding to 0.2μm gate length and open circles in Fig. 3a) is inversely proportional to the gate-length L_g and in agreement with the hydrodynamic results (dashed line in Fig. 3a) as shown in the Supporting Informations and those discussed above.** However, when the film of Y_2O_3 is thinner than 4nm, the plasma wave decays rapidly along the channel before a round trip is completed, which results in a weak dependence on the gate length L_g (solid squares in Fig. 3a).

By the way, the Y_2O_3 layer with 4nm thickness is sufficient for efficient gate-controlling even when the gate length shrinks down to 20nm. Actually in Fig. 3b, the plasma wave is overdamped along the channel of graphene FET with only 400nm gate-length if the dielectric layer is thinner than 8nm due to the enhanced screening of electrodes. As we discussed above, the ratio between gate length and dielectric thickness should not be too large, and the standing plasma oscillation prefers to be established along the 200nm channel (Fig. 3b). To indicate more clearly the effect of quantum capacitance, we mainly focus on the graphene FET with 200nm gate length and 4nm dielectric layer. **Here, the contribution of quantum capacitance is taken into account under different voltages following the discussed results of Fig. 1, from where the chemical potential μ is determined with the linear DoS distribution of pristine graphene. Therefore, the quantum correction is naturally included in n_s~$C_{TG}(C_{ox}, C_Q(\mu))V_{TG}$.** Due to the quantum capacitance effect, one can see the significant deviation of plasma resonances (open symbols in Fig. 3c) from those considering only the geometrical capacitance **(in this case the quantum capacitance is neglected, i. e. C_Q~0μF/cm^2 which is corresponding to the solid symbols in Fig. 3c)**. Besides, under the same gate voltage, the frequency of plasma resonance exhibits deviation over 1THz from the one without quantum correction. **Following this trend, it can be expected that the voltage dependence of plasma resonance will depend more evidently on the quantum capacitance in** mid-infrared nano-devices. The frequency of plasma resonance versus gate voltage V_{TG} can be modeled by a power law of the following type $f \propto V_{TG}^{\alpha}$. By fitting the data (dashed lines) of Fig. 3c, we extract α~0.5 in the device dominated by the geometrical capacitance (solid squares). With the quantum correction (open squares), it is found that the plasma resonances can be tuned in wider spectral region following the relationship $f \propto V_{TG}^{0.8}$. In view of this relation, it is inspiring to scale down the graphene FET with the aim to realize plasma-wave device with wide-tunability since most of graphene devices available now (e. g. disk, sheet arrays[24]) can be tuned approximately following $V_g^{0.25}$ relation.

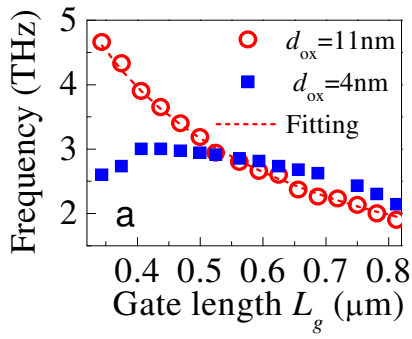

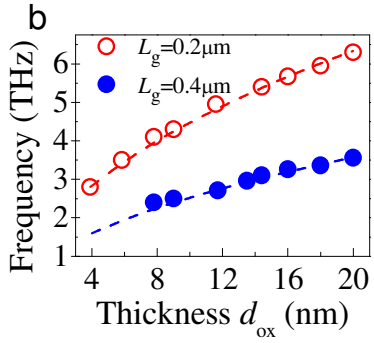

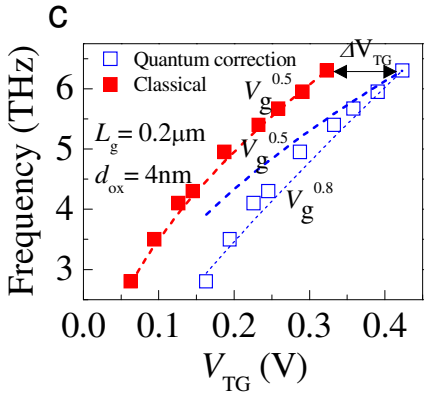

Fig. 3. The dependence of plasma resonance in quantum-capacitance dominated graphene FETs on the gate length L_g, dielectric-oxide (Y_2O_3) thickness d_{ox} and gate voltage V_{TG}. (a) The dependence of fundamental plasma resonance a on the gate length with dielectric Y_2O_3 thickness, d_{ox} =11nm (open circles) and 4nm (solid squares), respectively. The dashed line is the theoretical estimation based on the hydrodynamic model (seeing Supporting Informations), in agreement with the numerical results of FDTD (open symbols) based on the Kubo theorem. However, the FDTD data (solid squared symbols) exhibits significant deviation from L_g^{-1} rule due to the overdamping of plasma wave along the channel with only 4nm oxide. The oxide thickness d_{ox} dependence (symbols with FDTD solution) of plasma wave is shown in (b), where the predicted results of hydrodynamic theory are shown in dashed line with gate length L_g~0.4μm (blue line) and 0.2μm (red line). It can be found clearly that the vertical scaling behavior of plasma resonance continues when the relationship $\tau_{RC}<\tau$ holds, implying that the discharging time should be much shorter than the electron relaxation during the propagation of plasma wave. Thus, the plasma wave is almost overdamped in 0.4μm device when oxide layer is thinner than 8nm. (c) The frequency dependence of plasma resonance on the gate bias voltage V_{TG}, solid symbols are the frequency shift based on the classical capacitance, where the frequency is approximately proportional to $V_{TG}^{0.5}$. But, the quantum capacitance effect causes significant shift of plasma resonance to higher gate-voltage, and instead of the $V_{TG}^{0.5}$ relation, the frequency of plasma resonance follows approximately $V_{TG}^{0.8}$ relation.

To further analysis the effect of quantum capacitance, the comparisons on the voltage V_{TG} dependence of plasma resonance between 0.4μm (open symbols) and 0.2μm (solid symbols) gate length are made in Fig. 4a. It can be visualized clearly that the frequency of plasma resonance departures from $V_{TG}^{0.5}$-dependence (dashed lines in Fig. 4a) especially when the Fermi-level is close to the Dirac point (depicted by green dashed-circles). At this point, the quantum capacitance dominates over the geometrical capacitance due to its low DOS in graphene [25]. The shift of plasma resonance over 3THz in 0.2μm gate length is larger than the intrinsic resonant broadening $1/\tau$(seeing Fig. 2c), which ensures the observability of the predicted effects since the plasma resonance is more sensitive to the distribution of DOS if the device is scaling down for higher frequency application like mid-infrared or visible-light. In addition, in this Letter, we report that the quantum capacitance can also be obtained based on the plasma resonance except the electrostatic method described above. Following the dispersion relationship of plasma resonance (seeing Supporting Information), the Fermi-level E_F under different gate voltage V_{TG} can be deduced, and the capacitance-voltage (C_{TG}-V_{TG}) relationship can also be obtained supposing the linear dependence of DOS on E_F. It can be found in Fig. 4b that there is well consistent between theoretical (dashed lines) and experimental (symbols) results above the Dirac point.

So far, we mainly focus on the plasma resonance in pristine graphene sheet with linear DOS distribution near Dirac point. However, the many-body effects due to Coulomb interaction or resonant impurities can have profound impact on the quantum behavior of electron gas near Dirac point, which may results in the change of dynamical screening and plasma dispersion[26]. In this work, we consider only the case that the graphene sheet is adsorbed with low Ag-atom concentration, as shown in Fig. 4c. It has been known that the transport properties of graphene are not deteriorated when the concentration of adsorbed Ag atoms is sufficient low[27]. The results of density functional theory (Fig. 4e) also confirms that Ag-adatoms are resonant impurities rather

than long-rang Coulomb impurity with the dispersionless energy-level near Dirac point due to the repulsion caused by the adsorbate-host coupling, in well consistent with those predicted previously[27]. Because of this, a resonance maximum of C_{TG}-V_{TG} at Dirac point appears confirming again the modification of the DOS distribution due to Ag adatoms (Fig. 4d). In a strongly correlated electron system under strong magnetic field[1], a negative quantum capacitance emerges near the Dirac point of pristine graphene due to fractional quantum hall state. Even though the results in Fig. 4d do not exhibit the "negative compressibility", it is still reasonable to mimic the behavior in related to the strongly correlated system, as shown in Ref. 27. In Figs. 4d and 4e, above the Dirac point, the linear slope of DOS is almost unchanged, even when the concentration of Ag atoms increases up to 0.5% (the inset of Fig. 4d). Besides, both the total capacitance and DOS of the experimental results can be fitted well with that of pristine graphene above the Dirac point (seeing Figs. 4d and 4e).

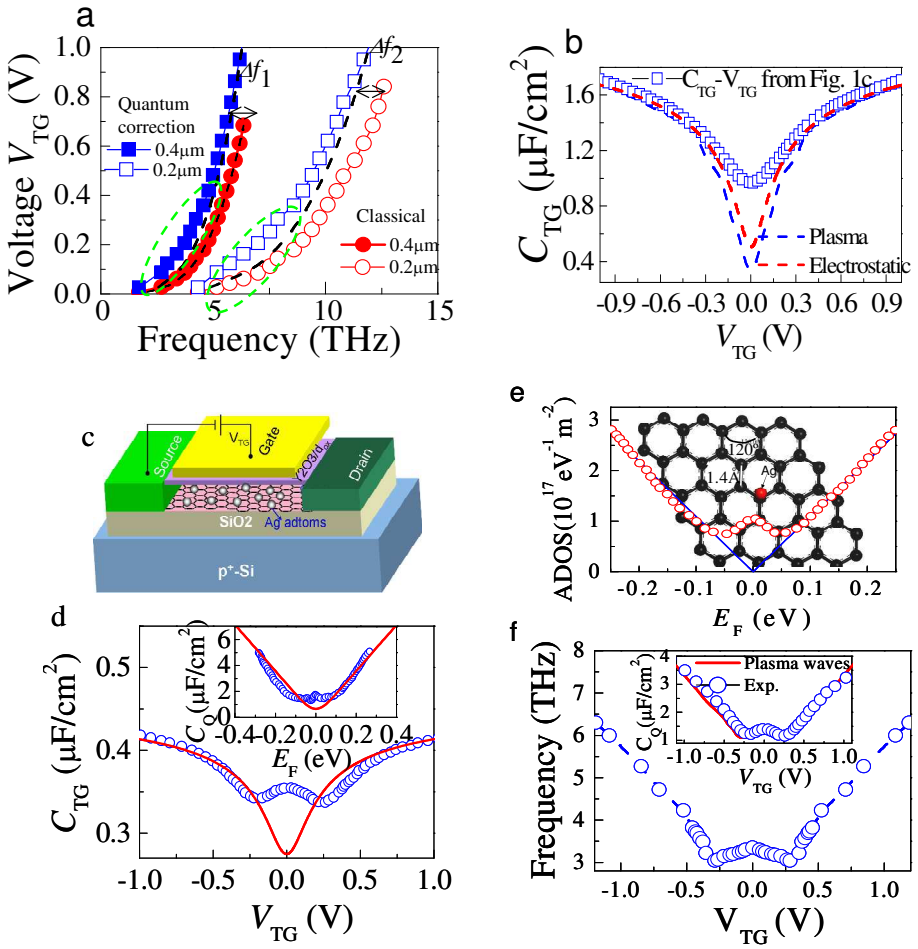

Fig. 4. The top-gate voltage V_{TG}-dependence of plasma resonance in grating-gated graphene FETs after considering the quantum-correction in pristine and Ag-adsorbed graphene sheets, and comparisons between experiments and relevant theories. (a) Voltage dependence of the fundamental plasma-resonance a as shown in Fig. 2 with gate length L_g~0.2μm (open symbols), 0.4μm (solid symbols) considering the contribution of quantum capacitance effect (solid and open squares) and only the geometrical capacitance (solid and open circles). The dashed lines follow the power law with $f \propto V_{TG}^{\alpha}$, and α~0.5 for the classical model. The dielectric layer thickness d_{ox} is

6nm. (b) Comparisons between C_{TG}-V_{TG} results measured by the capacitance bridge technique (open squares) and deduced from plasma dispersion in combination with FDTD results (blue dashed lines). The result based on the electrostatic model (red dashed line) is also shown for comparison. To indicate more clearly the effects of DOS distribution on the tunable plasma resonance, an Ag-adatom graphene FET is also considered (Fig. 4c). The experimental details can be found elsewhere[2]. The average DOS (ADOS) of the Ag-adsorbed graphene sheet is shown along with that of the pristine graphene (solid line) in Fig. 4e by the DFT calculation. In the meantime, C-V characteristic (open symbols) of Fig. 4d indicates the local maximum near the Dirac point, and converges to that of pristine graphene (red line) away from the Dirac point even though the Ag-adatom density is increased up to 0.5% in the inset. Following the Boltzman transport theory (seeing Supporting Informations), the frequency of plasma resonance is obtained in the Fermi-liquid regime, and the feature of resonance DOS is clearly visible in Fig. 4f.

Based upon above analysis, the high-frequency dynamics of Ag-adsorbed graphene is studied with the quasi-classical Boltzman transport theory in relaxation-time approximation[28] (seeing Sec. S3 in Supporting Informations). The frequency of plasma waves with 10nm Y_2O_3 dielectric layer under different gate voltages are shown in Fig. 4f, schematically. From the figure, it can be clearly seen the non-monotonously increasing of plasma wave frequency away from the Dirac point, where the resonant electronic state exists. The predicted phenomenon is counterintuitive since the free-electron absorption is usually thought to be proportional to the charge density in conventional plasmonic materials. It also reminds us the observation that plasma frequency of monolayer graphene is actually higher than that of bilayer one when the Fermi level is close to the Dirac point despite of higher DOS in bilayer graphene[30]. Therefore, even though the charge density is increasing continuously by tuning the Fermi level away from the Dirac point, the Drude weight is reduced when the fictions mass of charge grows faster than the charge density[31]. In other words, the Coulomb oscillation is weakening due to the inertia of plasma wave, which leads to the non-montonous plasma resonance near the Dirac point. The most interesting finding in Fig. 4f is that the frequency of plasma wave changes from sublinear to approximately linear dependence on the gate voltage. The results also indicate that the quantum capacitance has an important role in improving the tunability of plasma resonance in nanometer-sized graphene FETs. Furthermore, the total capacitance in the inset of Fig. 4d under different gate voltages can be reproduced well by following the dispersion relationship of plasma waves (seeing Supporting Informations).

In this Letter, another viewpoint for probing the quantum capacitance of graphene FETs is demonstrated in combination with the electromagnetic properties of plasma resonance. Through vertical scaling of graphene FETs, the tunability of plasma resonance can be improved due to the contribution of the quantum capacitance. The results presented are also applicable to the mid-infrared graphene plasmonics with various nano-patternings such as disk/nanoribbon arrays with the ionic-liquid gating, where the quantum capacitance also dominates. In the pristine graphene sheet, various quantum phases or non-Fermi-liquid behavior are observed at Dirac point[32]. And the renormalization of local DOS and energy band near the Dirac point or above provides insight into the features of different many-body excitations such as electron-plasmon and electron-phonon interactions[33, 34]. To those regards, the studying of plasma properties could turn out to be a very useful route to understanding the nature of electronic behavior at Dirac point. For example, our results are based on the usual Fermi-liquid state, where the Boltzman transport

theory or RPA approximation is applicable, and the emergence of new ground state may cause the departure of voltage dependence from that above Dirac point, as depicted in Fig. 4. On the other hand, the long wavelength limit of plasma resoance (see Supporting Informations) is applicable to the ground state of Wigner crystallization in low-density two dimensional Coulomb gas[35, 36], which possesses stability with respect to the small fluctuations about equilibrium position. And the compressibility of electronic-fluid like factional charged quasielectrons or quasiholes can sustained during the Coulomb interaction caused by the plasma resonance. In view of this, many-body interaction in strong correlated system may brings us a potential guideline to tailor the plasma effect of nano-metric graphene FETs for a wide spectrum of applications such as medical diagnostics, bionics and many other wide fields.

Methods

(i) Decorated-graphene device for C-V measurement: Top gated graphene FETs can be fabricated by graphene exfoliated from Kish graphite or CVD grown and placed on silicon substrate which is covered with a 300nm-thick SiO_2 layer[2,17]. A single-layer graphene can be identified by Raman spectroscopy measurements[11]. The devices can be defined by using electron-beam lithography and reactive ion or oxygen plasma etching[15]. As for the insulating Y_2O_3 film, a 3~6nm yttrium layer can be deposited firstly by using electron-beam evaporation followed by oxidation in air at ~180℃ for 30min to 60min. The thickness of Y_2O_3 film can be confirmed further by atomic force microscopy.

(ii) Plasmonic modeling technique: The Maxwell equations are solved by commercial-available software package EMW from Sentaurus-TCAD written in the FDTD algebra with the Kubo conductivity (seeing Supporting Information) embedded in the parameter file. The snap-shots of field-profile and time-domain signal are recorded to obtain the absorption/transmission spectra and plasma mode characteristics in Fig. 2. We carry density functional theory (DFT) calculation by using Vienna Ab initio Simulation Package (VASP) with the projector augmented wave basis sets, the relaxed geometry of Ag-adsorbed graphene and DOS distribution are calculated in Fig. 4. **We construct 4×4×1 supercell with sixteen carbon atoms and one Ag atom adsorbed on to one carbon atom as shown in the inset of Fig. 4e. The ground-state wave functions and eigenvalues are calculated by DFT/PBE functional of generalized-gradient approximation (GGA)[37] with a K-point grid of 4×4×1.**

ACKNOWLEDGMENTS

This work is supported in part by the State Key Program for Basic Research of China (2013CB632705, 2011CB922004), the National Natural Science Foundation of China (11334008, 61290301), the Fund of Shanghai Science and Technology Foundation (13JC1408800).

REFRENCES AND NOTES

[1]Brian, S.; Yu, G. L.; Geim, A. K.; Novoselov, K. S.; Shklovskii, B. I. Phys. Rev. B. **2013**, 88, 155417.

[2]Wang, L.; Chen, X.; Zhu, W.; Wang, Y.; Zhu, C.; Wu, Z.; Han, Y.; Zhang, M.; Li, W.; He, Y.; Wang, N. Phys. Rev. B. **2014**, 89, 075410.

[3]Kretinin, A.; Yu, G. L.; Jalil, R.; Cao, Y.; Withers, F.; Mishchenko, A.; Katsnelson, M. I.; Novoselov, K. S.; Geim, A. K.; Guinea, F. Phys. Rev. B, **2013**, 88, 165427.
[4]Xia, J.; Chen, F.; Li, J.; Tao, N. Nature nanotechnology, **2009**, 4, 505.
[5]Luryi, S. Appl. Phys. Lett. **1988**, 52, 501.
[6]Liu, H.; Si, M.; Deng, Y.; Neal, A. T.; Du, Y.; Najmaei, S.; Ajayan, P. M.; Lou, J.; Ye, P. D. **2014**, 8, 1031.
[7] Georgiou, T.; Jalil, R.; Belle, B. D.; Britnell, L.; Gorbachev, R. V.; Morozov, S. V.; Kim, Y.; Gholinia, A.; Haigh, S. J.; Makarovsky, O.; Eaves, L.; Ponomarenko, L. A.; Geim, A. K.; Novoselov, K. S. and Mishchenko, A. Nature Nanotechnology, **2012**, 8, 100.
[8]Xu, M.; Liang, T.; Shi, M. and Chen, H. Chemical Reviews, **2013**, 113, 3766.
[9]Yu, G. L.; Jalil, R.; Belle, B.; Mayorov, A. S.; Blake, P.; Schedin, F.; Morozov, S. V.; Ponomarenko, L. A.; Chiappini, F.; Wiedmann, S.; Zeitler, U.; Katsnelson, M. I.; Geim, A. K.; Novoselov, K. S. and Elias, D. C. Proc. Natl. Acad. Sci. USA **2013**, 110, 3282.
[10]Ye, J.; Craciun, M. F.; Koshino, M.; Russo, S.; Inoue, S.; Yuan, H.; Shimotani, H.; Morpurgo, A. F.; Iwasa, Y. Proc. Natl. Acad. Sci. USA **2011**, 108, 13002.
[11]Grigorenko, A. N.; Polini, M.; Novoselov, K. S. Nature Photonics, **2012**, 6, 749.
[12]Fernández-Rossier; Palacios, J. J.; Brey, L. Phys. Rev. B. **2007**, 75, 205441.
[13]Fang, Z.; Thongrattanasiri, S.; Schlather, A.; Liu, Z.; Ma, L.; Wang, Y.; Ajayan, P. M.; Nordlander, P.; Halas, N. J.; Javier García de Abajo, F. ACS Nano. **2013**, 7, 2388.
[14]Xu, H.; Zhang, Z.; Wang, Z.; Wang, S.; Liang, X.; Peng, L. ACS Nano. **2011**, 5, 2340.
[15]Fang, Z.; Wang, Y.; Schlather, A. E.; Liu, Z.; Ajayan, P. M.; García de Abajo, F.; Nordlander, P.; Zhu, X.; Halas, N. J. Nano Letters. **2014**, 14, 299.
[16]Xia, J.; Chen, F.; Li, J.; Tao, N. Nature nanotechnology, **2009**, 4, 505.
[17]Xu, H.; Zhang, Z.; Wang, Z.; Wang, S.; Liang, X.; Peng, L. ACS Nano. **2011**, 5, 5031-5037.
[18]Lee, J.; Chung, H.; Seo, D. H.; Lee, J.; Shin, H.; Seo, S.; Park, S.; Hwang, S.; Kim, K. Nano Research (in press) **2014**.
[19]Yan, H.; Li, X.; Chandra, B.; Tulevski, G.; Wu, Y.; Freitag, M.; Zhu, W.; Avouris. P.; Xia, F. Nature Nanotechnology. **2012**, 7, 330.
[20]Popov, V. V.; Polischuk, O. V.; Davoyan, A. R.; Ryzhii, V.; Otsuji, T.; Shur, M. S. Phys. Rev. B. **2012**, 86, 195437.
[21]Wang, L.; Hu, W.; Wang, J.; Wang, X.; Wang, S.; Chen, X.; Lu, W. Appl. Phys. Lett. **2012**, 100, 123501.
[22]Wang, L.; Chen, X.; Hu, W.; Yu, A.; Lu, W. Appl. Phys. Lett. **2013**, 102, 243507.
[23]Dyakonov, M.; Shur, M. IEEE Trans. Electron Devices, **1996**, 43, 380.
[24]Yan, H.; Li, X.; Chandra, B.; Tulevski, G.; Wu, Y.; Freitag, M.; Zhu, W.; Avouris, P.; Xia, F. Nature nanotechnology, **2012**, 7, 330.
[25]Das Sarma, S.; Li, Q. Phys. Rev. B, **2013**, 87, 235418.
[26]Gamayun, O. V. Phys. Rev. B, **2011**, 84, 085112.
[27]Wang, L.; Wang, Y.; Chen, X.; Zhu, W.; Zhu, C.; Wu, Z.; Han, Y.; Zhang, M.; He, Y.; Xiong, W.; Law, K. T.; Su, D.; Wang, N. Sci. Rep. **2013**, 3, 2041.
[28]Hwang, E. H.; Sarma, S. Das. Phys. Rev. B, **2009**, 79, 165404.
[29]Gamayun, O. V. Phys. Rev. B, **2011**, 84, 085112.
[30]Sensarma, R.; Hwang, E. H.; Sarma, S. Das Phys. Rev. B, **2010**, 82, 195428.
[31]Yoon, H.; Forsythe, C.; Wang, L.; Tombros, N.; Watanabe, K.; Taniguchi, T.; Hone, J.; Kim, P.;

Ham, D. Nature nanotechnology. **2014**, 9, 594-599.
[32]Brar, V. W.; Wickenburg, S.; Panlasigui, M.; Park, Cheol-Hwan; Wehling, T. O.; Zhang, Y.; Decker, R.; Girit, Ç.; Balatsky, A. V.; Louie, S. G.; Zettl, A.; Crommie, M. F. Phys. Rev. Lett. **2010**, 104, 036805.
[33]Krstajić, P. M.; Duppen, B. Van; Peeters, F. M. Phys. Rev. B. **2013**, 88, 195423.
[34]Walter, A. L.; Bostwick, A.; Jeon, K.; Speck, F.; Ostler, M. Phys. Rev. B. **2011**, 84, 085410.
[35]Chaplik, A. V. Zh. Eksp. Teor. Fiz. **1972**, 62, 746-753.
[36]Laughlin, R. B. Phys. Rev. Lett. **1983**, 50, 1395-1398.
[37]Perdew, J. P.; Burke, K.; Ernzerhof, M. Phys. Rev. Lett. **1996**, 77, 3865-3868.